Magnetic properties of the intercalated compound Lu₂Fe₃O₇

Sabreen S. Hammouda [1,2] Thomas Mueller [3] Eugen Weschke,[4] and Manuel Angst [1,*]

[1]*Jülich Centre for Neutron Science JCNS and Peter Grünberg Institut PGI,*
JARA-FIT, Forschungszentrum Jülich GmbH, 52425 Jülich, Germany
[2]*Lehrstuhl für Experimentalphysik IV C, RWTH Aachen University, 52056 Aachen, Germany*
[3]*Jülich Centre for Neutron Science JCNS, Heinz Maier-Leibnitz Zentrum (MLZ), Forschungszentrum Jülich GmbH,*
Lichtenbergstraße 1, 85748 Garching, Germany
[4]*Helmholtz-Zentrum Berlin für Materialen und Energie, Albert-Einstein-Strasse 15, D-12489 Berlin, Germany*

We have carried out a comprehensive investigation of the magnetic properties of the intercalated $Lu_2Fe_3O_7$ by the means of dc magnetization, polarized neutron scattering, and x-ray magnetic circular dichroism (XMCD) measurements. The results obtained by these techniques support a spin order in each of the Fe-O bilayers that is the same as observed in the nonintercalated $LuFe_2O_4$. In the Fe-O single layers, a magnetic moment appears to be induced by the application of a magnetic field, paramagnetic-like in the first approximation. Furthermore, a spin-charge coupling was revealed by the XMCD measurements.

I. INTRODUCTION

The rhombohedral layered compounds RFe_2O_4 (where R is a rare-earth metal) have attracted attention for 40 years, since interacting spin, charge, and orbital degrees of freedom on a lattice prone to geometrical frustration lead to a variety of unusual behaviors including anomalous thermomagnetization in $LuFe_2O_4$ [1], multiple successive phase transitions in YFe_2O_4 [2–4], and anisotropic dielectric dispersion in $ErFe_2O_4$ [5].

The ordering of the electronic degrees of freedom in RFe_2O_4 depends largely on the size of the rare-earth ion [6]. For Lu and Yb, which have almost the same ionic radius, very similar (Fe^{2+}/Fe^{3+}) charge and spin orders with $(\frac{1}{3}\frac{1}{3})$ in-plane propagation are established in the Fe-O bilayers [see Fig. 1(a)] [7–10]. For $LuFe_2O_4$, the charge order (CO) has been proposed to result in a new type of ferroelectricity [11], which attracted a lot of attention from researchers (for reviews see [6,12]). While the proposition of "ferroelectricity from charge ordering" in $LuFe_2O_4$ has been controversial [10,13–15], recent structural refinements on $YbFe_2O_4$ [8] indicate that the CO *does* involve polar bilayers, though with an antipolar stacking resulting in no net electric polarization.

In order to modify the CO, in particular the stacking of the CO in different bilayers, one can focus on the interactions between different bilayers, e.g., by inserting single Fe-O layers, increasing the distance between the bilayers; see Fig. 1(b). As the CO within individual bilayers of these "intercalated" rare-earth ferrites is expected to be very similar to that in non-intercalated compounds given the very similar local atomic arrangements [16], the intercalation possibly renders the antipolar stacking for $YbFe_2O_4$ [8] into a polar one. For the same

reasons, the spin order (SO) is also expected to be similar in the individual bilayers.

Oxygen off-stoichiometry (δ) inhibits the formation of long-range spin and charge order as observed for nonstoichiometric $LuFe_2O_{4\pm\delta}$ [7], $YFe_2O_{4\pm\delta}$ [17], and $YbFe_2O_{4\pm\delta}$ [9]. Moreover, variations in the magnetic behavior are found in dependence on the variations in oxygen stoichiometry [8,17–19]. In the same manner, for the intercalated compounds, we expect a dependence of the magnetic properties on the oxygen content as well.

Despite the potential of ferroelectricity in the intercalated compounds, understanding the magnetism in this system is missing; thus the spin-charge coupling is not yet verified to establish the corresponding multiferroicity. Moreover, the expected similarity of the spin order in the bilayers to the nonintercalated compounds still needs to be confirmed experimentally. Furthermore, the spin order in the additional single Fe-O layers and how it affects the magnetic ordering in this compound remain open questions. A clear picture of the magnetic ordering is missing due to the limited number of publications on intercalated ferrites [20–28]. Magnetic measurements, neutron diffraction, and Mössbauer spectroscopy studies [22,23,29] performed on off-stoichiometric polycrystalline $Lu_2Fe_3O_7$ indicate that the Fe-O single layer contains only Fe^{3+} ions, while the bilayer contains Fe with the same average 2.5+ valence as in $LuFe_2O_4$.

Here, we present extensive investigations of the magnetic behavior of $Lu_2Fe_3O_7$ single crystals using macroscopic magnetization measurements, polarized neutron scattering, and x-ray magnetic circular dichroism (XMCD). The various macroscopic magnetization measurements on $Lu_2Fe_3O_7$ suggest reduced magnetic correlations and the magnetic phase diagram is established. In polarized neutron scattering, a rod-like diffuse magnetic scattering extended along ℓ suggests correlations that are limited to the *ab* plane in the bilayers,
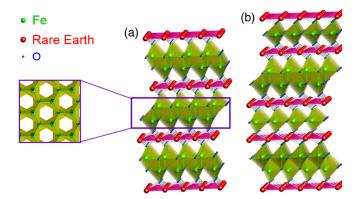
*m.angst@fz-juelich.de

FIG. 1. Crystal structure of (a) rhombohedral $LuFe_2O_4$ with three Fe-O bilayers in the unit cell, and (b) hexagonal $Lu_2Fe_3O_7$ with two Fe-O bilayers and one monolayer in the unit cell. The inset shows the projection of one bilayer in the ab plane.

which are still randomly stacked. A similar shape of the XMCD signal with a net magnetic moment of Fe^{2+} to that in $LuFe_2O_4$ is observed, indicating the same coupled spin-charge order in the individual bilayers as in the nonintercalated compounds.

II. EXPERIMENTAL PROCEDURE

We studied $Lu_2Fe_3O_7$ single crystals from [16] that were grown via the floating zone method in a CO_2/CO mixture to tune the oxygen partial pressure and subsequently the oxygen stoichiometry. These crystals are the following: the clearly oxygen-deficient single crystal called SC1 in [16], obtained from the crystal growth using a $CO_2 : CO = 50$ atmosphere, with a mass of 21.4 mg, showing a zigzag diffuse scattering; a less oxygen-deficient single crystal (SC2) with dimensions of $0.4 \times 0.2 \times 0.05$ mm^3 exhibiting incommensurate charge order; and a crystal closest to the ideal stoichiometry (SC3) with dimensions of $0.3 \times 0.18 \times 0.02$ mm^3 exhibiting a commensurate charge order. SC2 and SC3 were both from a growth using a $CO_2 : CO = 85$ atmosphere. A strong Ising behavior in the c direction is found in the magnetization measurements of [20]; therefore all the experimental procedures were done with $H \parallel c$. Macroscopic magnetization measurements were performed using the reciprocating sample option (RSO) of a Quantum Design magnetic property measurements system (MPMS) in fields up to 7 T for the small-size crystals SC2 and SC3 due to the high sensitivity (5×10^{-8} emu) especially in low fields, and the vibrating sample magnetometer (VSM) option of a Quantum Design PPMS (physical property measurement system) for the large sample SC1. Polarized neutron scattering was performed on SC1 at the DNS instrument at MLZ [30]. The x-ray magnetic circular dichroism (XMCD) measurements were performed in a magnetic field parallel to both the incoming beam and to the c axis at the Fe $L_{2/3}$ edges. The linear x-ray absorption spectra (LXAS) were performed at the O K edge for polarization parallel to the ab plane ($\vec{E} \parallel ab$) and polarization parallel to the c direction ($\vec{E} \parallel c$). Both the XMCD and the LXAS measurements were carried out on the beamline UE46/PGM-1 at the high-field diffractometer end station placed at BESSY II. In these measurements, the
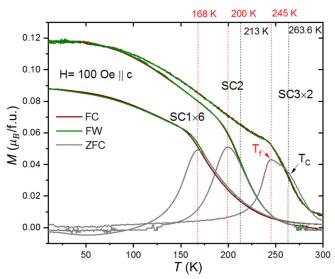

FIG. 2. Temperature dependence of magnetization measured with a field of 100 Oe applied parallel to the c direction during cooling (FC), warming (FW), and warming after zero-field cooling (ZFC) in a temperature range of 10–300 K for different $Lu_2Fe_3O_7$ single crystals. SC1 and SC3 are scaled for better visibility. T_C is assigned by the steepest slope in the FC curve, T_f by the maximum of the ZFC curve.

crystals were not cleaved and all the spectra were obtained in total electron yield (TEY) mode.

III. RESULTS

A. Macroscopic measurements

In our previous work on growth and preparation [16], we already found that the oxygen stoichiometry influences the magnetic behavior of $Lu_2Fe_3O_7$ crystals. This is confirmed by the temperature-dependent magnetization $M(T)$ performed in low magnetic fields on three different crystals SC1, SC2, and SC3, shown in Fig. 2. The shape of the low-field magnetization curves is similar to those in the literature, with the characteristic temperatures ($T_C \sim 264$ K, $T_f \sim 245$ K) of SC2 and SC3 being close to the lower [26] and higher [27] limits of the corresponding temperatures deduced from previously reported data. The magnetization after cooling to low temperatures in 100 Oe ($\sim$0.06 μ_B/f.u.) is in between the corresponding values discernible from previous results obtained in the same field, though closer to the lower value (0.46 μ_B/f.u. [28] and 0.03 μ_B/f.u. [27]). Studies on nonintercalated rare-earth ferrites [2,6,7,9,17,18] indicate that oxygen deficiency leads to a lowering of characteristic temperatures. Based on these results and the oxygen partial pressures used during synthesis [16] we determine that SC1 is the most oxygen-deficient crystal, while the oxygen content of SC2 ($M(T)$ of SC2 was shown before in [16] and is repeated here for comparison) is in between the ones of SC1 and SC3. The off-stoichiometric crystal SC1 was used for neutron diffraction due to its large size. In the following, we will focus on the magnetic properties of the stoichiometric SC3.

Figure 3(a) shows $M(T)$ data of SC3 measured in magnetic fields up to 7 T upon cooling and warming. The M (field

FIG. 4. $M(H \parallel c)$ loops measured on SC3 at different temperatures. Inset: Hysteresis loop including the virgin curve measured after cooling in zero field at 160 K.
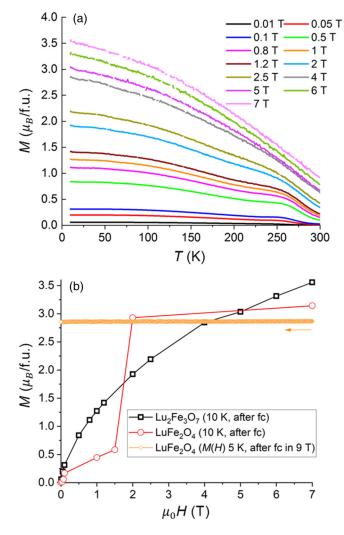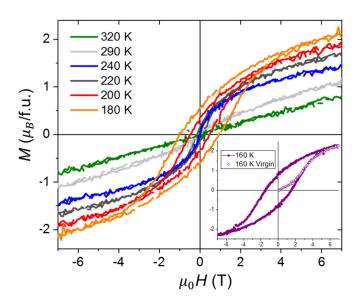

FIG. 3. (a) Temperature-dependent magnetization during field cooling and followed by field warming at different magnetic fields for SC3. FC, and FW perfectly overlap for all used fields. (b) Low-temperature magnetization obtained by cooling in different magnetic fields for $Lu_2Fe_3O_7$ (squares) and for $LuFe_2O_4$ (circles). For $LuFe_2O_4$ also shown (small diamonds) is $M(H)$ obtained in decreasing H after cooling in 9 T (taken from the full $M(H)$ loop shown in Fig. 4.5(b) in [18]).

cooling, FC) and M (field warming, FW) data overlap within error bars in all measured fields. With increasing H, the feature assigned T_C starts to smear out and shift to higher temperatures as expected for a ferro- or ferrimagnetic transition; the shift was noticeable as determined by the steepest slope criteria (see Fig. 6). For fields higher than 2 T, the peaklike shape below T_C vanishes and a continuous increase of the magnetization is observed. The net moment at low temperature, extracted from the field-cooling curves, is inconsistent with a ferromagnetic order (for which 10 μ_B/f.u. would be expected) and depends on the applied field as shown in Fig. 3(b).

For comparison, the low-T moment of $LuFe_2O_4$, extracted from field-cooled $M(T)$ data is also shown. Low values for cooling fields below 1.5 T are due to the sample not being in the ferrimagnetic phase anymore as is clear from the $M(T)$

curves (Fig. S2 in [31]). In contrast, whenever $LuFe_2O_4$ is in the ferrimagnetic phase, there is a nearly field-independent low-T moment of ~ 3 μ_B/f.u. This is particularly clear in $M(H)$ data measured in decreasing fields after cooling to 5 K in a sufficiently high field, in which case $LuFe_2O_4$ remains in the ferrimagnetic phase down to zero field. We therefore include in the figure also a corresponding measurement from a different $LuFe_2O_4$ crystal, the full $M(H)$ loop of which is shown in Fig. 4.5(b) in [18].

As can be seen, at low T $LuFe_2O_4$ containing only the Fe-O bilayers exhibits an approximately field-independent moment (as long as it is in the ferrimagnetic phase). In contrast, in low fields $Lu_2Fe_3O_7$ exhibits a clearly lower low-T moment, despite the absence of any additional transition to a different phase [compare Fig. 3(a) with Fig. S2]. It reaches a moment comparable to $LuFe_2O_4$ only at about 4–5 T, and interestingly continues to increase afterward with an approximately linear behavior in the moment-field dependence. This additional field dependence indicates the contribution of magnetic moments in the single layer, which are induced by the magnetic field, and like in a paramagnetic phase, the induced moments are apparently proportional to the applied field.

Figure 4 shows the hysteresis [$M(H)$] loops measured on SC3 at different temperatures. The shape of these loops below T_C corresponds to the behavior expected for ferro- or ferrimagnetic spin order. In contrast to the nonintercalated $LuFe_2O_4$ [18], no indications of a metamagnetic transition were observed; for example the virgin curve of the $M(H)$ loop (inset of Fig. 4) is within error bars inside the loop. The linear behavior at 320 K reveals a purely paramagnetic phase. However, at 240 K and above, $M(H)$ exhibits a nonlinear behavior with bending in the low-field region (S-like shape). Such a bending in $M(H)$ was previously observed in $LuFe_2O_4$ [18] in a wide T range above the transition temperature and it was attributed to short-range correlations in the individual bilayers [7,18]. Below 220 K, $M(H)$ exhibits
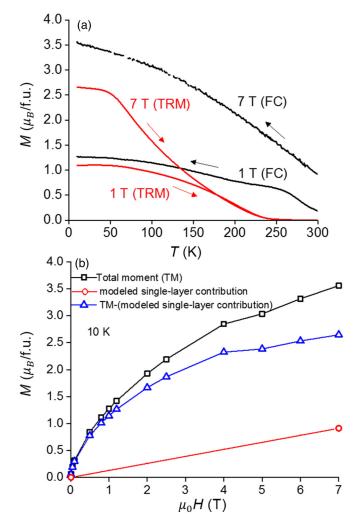
FIG. 5. (a) Temperature dependence of thermoremanent magnetization of $Lu_2Fe_3O_7$ after cooling in two different external fields with 2 K/min and the corresponding field-cooling curves. (b) Total moment at low temperature from Fig. 3(b) and linear fitting (red line) of FC-TRM (red circles). The subtraction of the modeled single-layer contribution from the total moment results in the tentative bilayer contribution (blue curve).

a hysteresis resembling a ferrimagnetic phase with remanent magnetization. All the measured loops do not reveal a saturation in fields up to 7 T, in agreement with the FC measurements shown Fig. 3(b). Note that we show here $M(H)$ data only at temperatures down to 160 K, because at lower temperatures our maximum field of 7 T is insufficient to close the hysteresis. The $M(H)$ loops shown in the literature were generally measured at 80 K [24–27], often up to fields too low to close the hysteresis and sometimes interpreted in terms of exchange bias. The $M(H)$ measured up to 15 T [26], nearly enough to fully close the hysteresis, has a shape very similar to the one of our measurement at 160 K (inset).

Figure 5(a) shows thermoremanent magnetization (TRM) measurements, which were carried out by measuring upon warming from 10 K to 400 K in zero field after the sample had been cooled to 10 K in either 7 T or 1 T. The corresponding FC curves are also shown. Unusually large TRM values are noticeable at low T. Such unusually large values have been

observed previously in $LuFe_2O_4$ with almost no difference to the FC value at the base temperature, attributed to the system being trapped in a high-field phase. For temperatures below $\sim$60 K, a plateau behavior can be seen. This is similar to what was observed in $LuFe_2O_4$ [18,32,33] and also in a few other systems [34,35]. The explanation for this behavior in $LuFe_2O_4$ [18] was in terms of "kinetic arrest," in which the magnetic phase in the system is trapped in a metastable phase and the transition to a more thermodynamically stable phase by cooling in low field is prohibited by a barrier exceeding the thermal fluctuations. This can be seen in the drop of the TRM curve upon continuous warming through a freezing temperature around 60 K. However, in $Lu_2Fe_3O_7$ the drop in magnetization is gradual and less sharp compared to $LuFe_2O_4$ due to the sample inhomogeneity. We note that the remanent magnetization after cooling to low temperature in 1 T is about twice as large as the one previously [26] reported after cooling in the similar field of 1.1 T, and the TRM of $Lu_2Fe_3O_7$ reaches zero at around $\sim$245 K, comparable to previous reports [25,26]. A significant difference in the magnetization at low temperature between the FC and the corresponding TRM can be seen compared to $LuFe_2O_4$. This difference is very large, particularly after cooling in 7 T. After cooling in the higher fields, the TRM exhibits $\sim$2.7 μ_B per formula unit, which is very close to that for $LuFe_2O_4$ (2.9 μ_B/f.u.) [18]. This was also observed before in $Lu_2Fe_3O_7$ by [26]. This observation is consistent with similar spin arrangements in the bilayer to those in $LuFe_2O_4$. The difference between FC and TRM at low temperature for 7 T is about 7 times larger than the value for 1 T; therefore, the net magnetic moment aligned in the field direction could be assumed to be purely induced by the magnetic field, i.e., paramagnetic. Thus, no contribution from the single layer for the TRM exists. This suggests that the additional 1 μ_B per formula unit in the FC of $Lu_2Fe_3O_7$ in 7 T at low temperature compared to $LuFe_2O_4$ is from the single layers. To extract the tentative bilayer contribution [see Fig. 5(b)] at low temperature, the single-layer contribution was estimated as the difference between FC and TRM and modeled as "paramagnetic" ($M \propto H$), then subtracted from TRM.

Figure 6 represents the tentative magnetic "phase" diagram for $H \parallel c$ established from $M(T)$ and $M(H)$ measurements. The phase diagram includes four different "phases": paramagnetic (PM), 2D-fM (ferrimagnetic), cluster glassy phase (CG), and the region of kinetic arrest. The "phase boundary" between paramagnetic (PM) and ferrimagnetic (fM) is determined by the steepest (maximum) slope in the FC measurements (T_C) [Fig. 3(a)]. It is remarkably similar to that reported for $LuFe_2O_4$ [18,33]; however, in $Lu_2Fe_3O_7$, the ferrimagnetic state is not long-range ordered in contrast to $LuFe_2O_4$, and therefore strictly speaking not a thermodynamic phase. Switching between PM and fM can be achieved directly by cooling or warming in H because FC and FW are overlapped and no thermal hysteresis is present. Applying a magnetic field shifts the corresponding temperature to higher values. However, nonlinear $M(H)$ measurements in the PM phase provided indications of internally ordered bilayers that are randomly stacked in light of similar evidence discussed for $LuFe_2O_4$ [18].

The "phase boundary" between fM and the cluster glassy phase (CG) is determined by the maximum of the zero-field-
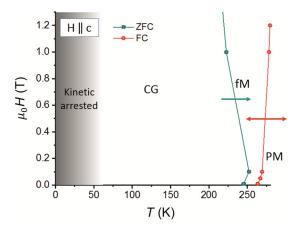
FIG. 6. H-T "phase" diagram for SC3 of $Lu_2Fe_3O_7$ extracted from different DC measurements. Three magnetic "phases" are labeled PM, fM, CG; see text for labeling. The red circles were obtained from the FC measurements in different fields and the cyan squares from ZFC measurements in different fields. Arrows indicate the direction of the temperature change for which a feature occurs. The blurred blue area indicates that the transition CG-fM is arrested below ~60 K.
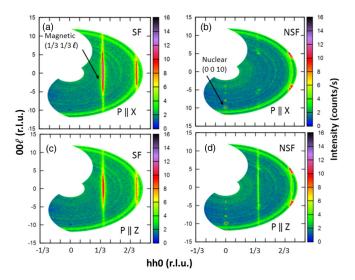

FIG. 7. Neutron scattered intensity in the $(hh\ell)$ plane at 4.2 K in spin-flip [(a), (c)] and non-spin-flip [(b), (d)] with neutron polarization (a), (b) parallel to $\vec{Q}$ direction and (c), (d) perpendicular to scattering plane for five detector positions and counting time 24 s each position (sample SC1). When the polarization of the neutrons is parallel to the scattering vector, both in-plane and out-of-plane components of the magnetic contribution are measured in the spin-flip (SF) channel and the full nuclear coherent contribution is measured in the non-spin-flip (NSF) channel, i.e., structural reflections (00ℓ) with $\ell = 2n$.

cooling (ZFC) measurements (T_f) (see Fig. S1 in [31] for ZFC measurements). The fM region likely corresponds to short-range magnetic order as is indicated by the absence of any sharp feature in the FC curve in low H. Thus, no long-range order is present and a freezing of the spins only occurs in the H-T region labeled CG. This CG phase likely originates from the presence of single Fe-O layers, which unavoidably modifies the coupling between the different bilayers to be weaker compared to $LuFe_2O_4$, thus preventing long-range spin correlations between different bilayers and ultimately the establishment of 3D long-range order. Upon further cooling to temperatures below ~60 K, the system appears to be kinetically arrested indicated in the figure by the blurred gray area. The blurring should indicate the uncertainty of the characteristic temperature for kinetic arrest determined from the drop in the thermoremanent data [Fig. 5(a)].

B. Polarized neutron scattering

More details about the spin arrangement can be obtained by scattering methods, in particular neutron scattering. Unfortunately, the previously discussed SC3 is too small for neutron scattering, whereas larger crystals including SC1 (see Fig. 2) were found to be off-stoichiometric and exhibit only diffuse magnetic rodlike scattering along $(\frac{1}{3}\frac{1}{3}\ell)$ shown in Fig. 7, as previously observed in [20,22]. However, additional information (e.g., the moment direction) can be obtained with polarized neutron scattering. Therefore, polarization analysis was used to explore the spin anisotropy, since a reduction of the anisotropy was observed in the diffuse magnetic scattering slightly above the Néel temperature in nonintercalated YFe_2O_4 [4].

Figure 7 shows the mapped $hh\ell$ plane of SC1 at 4.2 K for the different polarization directions. To separate magnetic scattering from nuclear scattering [36], a neutron polarization parallel to the average $\vec{Q}$ was used ($\vec{P} \parallel \vec{x}$); see panels (a)

and (b). In this orientation, all the magnetic scattering will involve a spin flip regardless of the moment orientation. The weak diffuse peak at $\sim(\frac{1}{3}\frac{1}{3} \pm 5.5)$ in the non-spin-flip channel for $\vec{P} \parallel \vec{x}$ [Fig. 7(b)] must be of structural origin and may be due to medium-range CO, which appears more 3D than 2D (note that peaks at these positions were also observed in neutron diffraction of $LuFe_2O_4$ and attributed to CO [37]). The nature of peaks rather than the lines of diffuse scattering apparent in the spin-flip channel [Fig. 7(a)] suggests that there are significant correlations of CO between different bilayers.

Clearly, magnetic diffuse scattering is observed in the spin-flip scattering [Fig. 7(a)] that is relatively sharp in the $hh0$ direction but extended along ℓ, indicating that the spin correlations are mostly limited to the ab plane with disorderly stacked bilayers. Since the distance of iron ions in different bilayers is much larger than the in-plane nearest-neighbor distance (cf. Fig. 1), in-plane correlations are much stronger than out-of-plane correlations. The appearance of only diffuse scattering suggests that the crystal is at least not stoichiometric enough to exhibit long-range spin order, rather exhibiting a cluster-glass-like freezing.

To determine the orientation of the modulated spins, additional measurements with polarization perpendicular to the scattering plane ($\vec{P} \parallel \vec{z}$) were performed; see panels (c) and (d). In this configuration, the spin-flip (SF) channel is sensitive to the magnetic moment in the $(hh\ell)$-scattering plane, while the moments perpendicular to the scattering plane give rise to magnetic scattering in the non-spin-flip (NSF) channel. The additional intensity observed in the non-spin-flip channel for $\vec{P} \parallel \vec{z}$ [Fig. 7(d)] compared to $\vec{P} \parallel \vec{x}$ [Fig. 7(b)] indicates the presence of magnetic moments pointing out of the scattering

plane, and thus perpendicular to the crystallographic c axis of $Lu_2Fe_3O_7$.

To calculate the in-plane and out-of-plane modulated spin components for the Fe ions, the NSF ($\vec{P} \parallel \vec{x}$) was subtracted from NSF ($\vec{P} \parallel \vec{z}$). The subtraction is done to get rid of the nuclear scattering, which is present in both channels, and to obtain the magnetic scattering from the modulated spin components perpendicular to the scattering plane, i.e., in the $\bar{1}10$ direction (this is only present in NSFz). Then, the intensity of the diffuse scattering was averaged along ℓ in the range $\ell = -5$ to $\ell = 5$ for NSFz after the subtraction and for the SFz channels. Finally, a numerical integration along the $hh0$ direction was performed on both SFz and NSFz channels resulting in intensity values of 0.0591 counts/s · r.l.u. for NSFz and 0.225 counts/s · r.l.u. for SFz. The ratio of the corresponding spin components (scaling with the square root of the intensities) of 001 ($\parallel c$) to $\bar{1}10$ directions is 0.47/0.24 $\sim$ 2. The macroscopic measurements in Fig. 3(d) indicated a similar SO in the bilayer as in the nonintercalated compound, implying that both Fe^{2+} and Fe^{3+} spins in the bilayers point into the c direction. The Fe^{2+} spins are aligned $\parallel c$ due to the crystal field and spin-orbit coupling and the bilayer Fe^{3+} spins are coaligned by the exchange interaction with the Fe^{2+} spins. The bilayer contains twice the spins that exist in the single layer and therefore the single-layer contribution to the intensity would be expected to be half of the one in the bilayer, which coincides with the obtained ratio of $\sim$2. Assuming the contribution to the moments is roughly proportional to the number of spins, this suggests that the single-layer spins are modulated in-plane completely. With such an in-plane antiferromagnetic order, a not too large magnetic field applied out-of-plane is expected to induce an out-of-plane net moment that is proportional to the field [38], consistent with our observations (Sec. III A). Furthermore, our deduced primarily in-plane orientation of the modulated single-layer spins is consistent with the conclusions from Mössbauer spectroscopy [29], in which single-layer spins pointing into a direction just 20° from the plane were found.

Figure 8 shows the ℓ dependence of the intensity (averaged along $hh0$ from $h = 0.25$ to 0.4) of the diffuse magnetic scattering in the spin-flip channel ($\vec{P} \parallel \vec{z}$). The smoothed peak is extremely broad, demonstrating that the data is consistent with almost no spin correlations in the c direction. For comparison, the magnetic intensity is modeled for randomly distributed Fe^{2+} and Fe^{3+} spins with the Ising spins pointing along the c axis according to

$$I_{\mathrm{model}} = f_m{}^2 \times P(\alpha)^2 \times \mathrm{DWF}^2, \quad (1)$$

where $P(\alpha) = \arccos(\alpha)$, α being the deviation angle of the scattering vector $\vec{Q}$ from the magnetization $\vec{M}$, is the direction factor. The direction factor leads to a suppression of the measured intensity along ℓ, as does the magnetic form factor $f_m(Q)$. DWF $= \exp(-\mathrm{DW} \cdot \vec{Q}^2)$ is the Debye-Waller factor, with DW $= 0.006$ Å^2 according to the refinement of the crystal structure at 100 K (no 4.2 K data are available) from x-ray diffraction. The modeled intensity was calculated twice—including and excluding the DWF—and is shown in Fig. 8. As can be seen, there is no significant influence of the DWF on the modeled intensity. The modeled intensity is slightly broader than the smoothed measured data; the reason
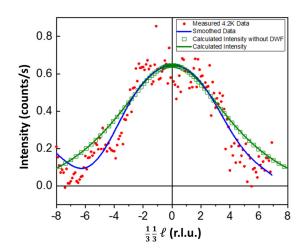

FIG. 8. Diffuse magnetic scattering at the $(\frac{1}{3}\frac{1}{3}\ell)$ line (intensity averaged along $hh0$ from 0.25 to 0.4) in the spin-flip channel for neutron polarization parallel to $\vec{z}$ direction at 4.2 K. The smoothed data (blue) and the intensity model for the random distribution of Fe^{2+} and Fe^{3+} (green line, squares: with, without Debye-Waller factor) are also shown. Background is subtracted for the measured data.

behind this may be that the modeled intensity does not take into account any present correlation even within the bilayers besides instrumental resolution and mosaicity.

Figure 9(a) shows the in-plane dependence of the intensity (averaged along ℓ from $\ell = -5$ to $\ell = 5$) of the diffuse magnetic scattering (spin-flip, $\vec{P} \parallel \vec{x}$) at different temperatures. These were fitted with Lorentzians (solid lines), and the inset shows the T dependence of the corresponding peak maxima (full diamonds) and areas (full circles). For comparison, the inset also shows the peak intensities reported by [20] (open squares) and [22] (open diamonds). While at elevated temperatures the T dependence of our integrated intensity is fairly close to those previous reports, the peak maxima decrease more quickly upon warming, extrapolating to zero at about 250 K rather than 300 K. This suggests that the correlations in our sample SC1 are destroyed faster by thermal fluctuations. This may be expected given that the $M(T)$ curves of Fig. 2 also show significantly reduced characteristic temperatures for sample SC1.

The extracted full widths at half maxima (FWHMs) were corrected by subtracting the instrumental resolution (0.0066 r.l.u.) and are shown in Fig. 9(b). The FWHM is significantly larger than the one reported by [20] (assuming they use the same units), which like the reduced temperature scale we attribute to a larger oxygen deficiency of sample SC1. The corresponding in-plane correlation lengths were obtained as $\xi = 2/\mathrm{FWHM}$ and are shown in Fig. 9(b). Note that sample SC3, which was too small for neutron scattering but is much less oxygen deficient, likely has significantly larger correlation lengths.

Interestingly, anomalies around 60 K exist in the T dependencies of both the FWHM and the peak intensity. Such an anomaly is also visible in the peak intensities reported by [20] (though not in those of [22]). The anomaly was tentatively attributed to an ordering of Fe^{3+} spins in the single layers [20]. The fact that the corresponding anomaly in our sample SC1
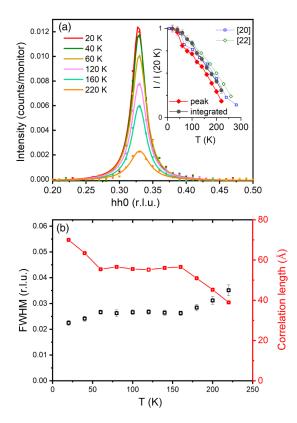
FIG. 9. (a) Diffuse magnetic scattering averaged along the ℓ direction in the range $\ell = -5$ to $\ell = 5$ in the spin-flip channel measured with $\vec{P} \parallel \vec{Q}_{average}$ vs $hh0$ for selected temperatures. The data were fitted with a Lorentzian (solid curves) and the background is subtracted for all curves. The inset shows the temperature dependence of both integrated and peak intensities. The peak intensities of [20,22] are also shown for comparison. (b) Correlation length and full widths at half maxima extracted from the data fitting for various temperatures.

[Fig. 9(a) inset, full diamonds] is less pronounced than the one observed in [20] (open squares) indicates that such a full or partial ordering of the single-layer spins at low T is also hindered by oxygen deficiency, as may be expected. The estimated correlation length in the $hh0$ direction at 100 K is $\sim16a$. This is larger than the correlation length along ℓ. However, it is much smaller than the estimated correlation length for $LuFe_2O_4$ below T_N ($\sim73a$ [18]), though slightly larger than the estimated correlation length above T_N ($\sim13a$ at 260 K [18]).

C. X-ray magnetic circular dichroism

As Lu^{+3} is nonmagnetic, the magnetism arises from contributions of the Fe ions both in the single Fe-O layers and in the Fe-O bilayers (cf. Fig. 1). However, the Fe ions have two valance states. Therefore, XMCD measurements were carried out due to their ability to deduce the spins belonging to the different valences in the same way previously done on $LuFe_2O_4$ [10,39,40]. No XMCD measurements were reported before on intercalated rare-earth ferrites. The measurements were performed on SC3 at the same temperature as $LuFe_2O_4$ had been measured for comparison, i.e., 120 K [10]. This
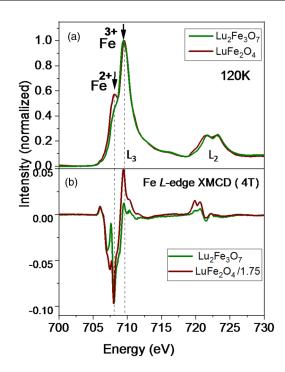

FIG. 10. (a) XAS spectrum [XAS $= (\mu_- + \mu_+)/2$] of stoichiometric $Lu_2Fe_3O_7$ and $LuFe_2O_4$ crystals in a field of 4 T normalized to the peak maximum. (b) The corresponding XMCD signals [XMCD $= (\mu_+ - \mu_-)$]. The $LuFe_2O_4$ XMCD signal was taken from [18] and scaled through division by 1.75.

temperature had been chosen for $LuFe_2O_4$ because it is the lowest temperature at which the sample was conductive enough for TEY, and avoiding the charging effect in the insulating phase [40].

In addition, linearly polarized x-ray absorption measurements at the O K edge were performed to determine the possible orbital moment contribution [40] and to study the effect of the presence of the single-layer Fe^{3+} (see Fig. S3 in [31]).

Figure 10(a) shows the normalized x-ray absorption spectra (XAS) for SC3 of $Lu_2Fe_3O_7$ and $LuFe_2O_4$. The latter was taken from [10]. The corresponding XMCD signals are shown in panel (b). Two peaks can be discerned in the XAS at the L_3 edge; these peaks are assigned to Fe^{2+} and Fe^{3+} according to the XAS spectrum and the XMCD signal of $LuFe_2O_4$. In the XMCD signal a large downward peak at ~708 eV and a smaller upward peak at ~709.5 eV are visible. A downward (upward) peak in the XMCD at the L_3 edge corresponds to a net magnetic moment pointing into (opposite to) the field direction. Thus, one can conclude that the net magnetic moment of the Fe^{2+} ions is in the field direction and the net magnetic moment of the Fe^{3+} ions opposite to the field direction. Moreover, the downward Fe^{2+} peak is much larger than the positive Fe^{3+} peak. Given that Fe^{2+} has a spin value of 2 while Fe^{3+} has a larger value of 5/2, and neglecting the orbital magnetic moment of Fe^{2+}, this implies that not all the Fe^{3+} spins point opposite to the field. In the XAS, the Fe^{2+} peak (more like a shoulder) has less height than the Fe^{3+} peak, similar to what was observed in $LuFe_2O_4$ [10,18]. In [10,18], the peak height difference was explained as due to surface

oxidation, because TEY is very surface sensitive. The surface oxidization effect on the XAS had been verified by performing the measurements in fluorescence yield, which is more bulk sensitive, and indeed a Fe^{2+} : Fe^{3+} ratio close to 1 had been observed in fluorescence yield [10,18]. Moreover, for *in situ* cleaved crystals of $LuFe_2O_4$, a peak ratio in the L_3 region close to 1 was observed [39] (the crystals measured here and in [18] were not cleaved). However, while the x-ray absorption spectrum (XAS) was found to be affected by surface oxidization in $LuFe_2O_4$, no significant influence on the XMCD was found, indicating that the affected thin surface layer is nonmagnetic [10,39,40]. Apart from this surface effect, the Fe^{2+} contribution is further reduced in $Lu_2Fe_3O_7$, because per formula unit, one Fe^{2+} ion of three Fe ions contributes to the XAS in $Lu_2Fe_3O_7$ whereas one Fe^{2+} ion of two Fe ions contributes to the XAS in $LuFe_2O_4$.

The two XAS curves look different, which may be attributed to the presence of the additional Fe^{3+} single layer in $Lu_2Fe_3O_7$. However, both compounds exhibit a similar XMCD spectral shape. In Fig. 10(b), the shown XMCD signal of $LuFe_2O_4$ is scaled through division by a factor of 1.75 for comparison with $Lu_2Fe_3O_7$. This factor is chosen such that the negative Fe^{2+} peak maximum of both compounds is the same. Both the XMCD and XAS signals are normalized with respect to the maximum of the XAS peak. The XAS maximum is proportional to the amount of Fe/f.u. $LuFe_2O_4$ contains 2 Fe ions (one Fe^{2+} and one Fe^{3+}) per formula unit, whereas $Lu_2Fe_3O_7$ contains 3 Fe ions (one Fe^{2+} and two Fe^{3+}) per formula unit. Therefore, the XMCD is normalized with respect to the amount of Fe (Fe^{2+} and Fe^{3+}) ions leading to a scaling factor of 1.5 ($\frac{1}{3}/\frac{1}{2}$) and with respect to Fe^{3+} ions leading to scaling factor of 2 ($\frac{1}{2}/1$). These two possibilities for the normalization were considered because it is not clear how much Fe^{2+} contributes to the peak at the nearby Fe^{3+} position. However, a scaling factor of 1.75 might indicate that not all Fe^{2+} ions contribute to the XAS maximum or it might in part also be because the material is not saturated at 4 T [cf. Figs. 3(a) and 4].

As discussed above, in $Lu_2Fe_3O_7$ the Fe^{3+} net moment is smaller than the Fe^{2+} net moment and is pointing in the opposite direction (negative H direction). We now consider the 1/3-type spin order similar to $LuFe_2O_4$, which basically implies that three independent Fe^{2+} spins are present. This spin model has all the Fe^{2+} and $\frac{1}{3}$ of the Fe^{3+} spins aligned in the field direction and $\frac{2}{3}$ of the Fe^{3+} spins aligned opposite to the field direction [8]. One can conclude that all Fe^{2+} spins are pointing in one direction since a scaling factor of 1.75 (close to 1.5) was used and this leads to a comparable Fe^{2+} peak taking into account the XAS normalization [Fig. 10(b)]. We note that for $LuFe_2O_4$, a significant orbital magnetic moment was concluded from the sum rules for Fe^{2+} [10,13,39–41], which brings the overall magnetic moment closer to the one of Fe^{3+}. This is very likely also the case for $Lu_2Fe_3O_7$, but we refrain from reporting the corresponding sum rule analysis due to the large error bars found. In contrast, the Fe^{3+} net moment is clearly much smaller in $Lu_2Fe_3O_7$ compared to $LuFe_2O_4$. In $Lu_2Fe_3O_7$, the Fe^{3+} negative net moment arises from two contributions: (1) the net moment from Fe^{3+} in the bilayer and (2) the net moment from Fe^{3+} in the

single layer. Thus, the much smaller overall negative Fe^{3+} net moment may be due to a smaller negative bilayer-Fe^{3+} net moment or due to a positive net moment in the single layer or due to a combination of these effects. The most likely scenario is that the bilayer arrangement is identical to $LuFe_2O_4$ [10,18], and the smaller Fe^{3+} positive peak in XMCD is due to the single-layer spins (partially) polarized in the H direction, as also indicated by the macroscopic measurements.

IV. DISCUSSION AND CONCLUSION

Generally, the studied $Lu_2Fe_3O_7$ crystals exhibit a magnetic behavior that is similar to $LuFe_2O_4$. Many common features are observed: (1) the Ising spin behavior along the c direction observed in the macroscopic magnetization measurements [7,37]; (2) the temperature range where magnetic ordering or freezing occurs (~200–250 K) [7,37]; (3) the $\frac{1}{3}\frac{1}{3}$ in-plane propagation observed in diffuse magnetic scattering or Bragg peaks [7,42]; (4) the presence of the thermoremanent magnetization (TRM) with the unusually high TRM starting to drop to lower values only upon warming above ~50 K, which may be accounted for by kinetic arrest [18]; (5) the deviations from paramagnetic linear behavior in $M(H)$ above T_C [7]; (6) the shape of the XMCD signal with a large downward peak at the Fe^{2+} position and a smaller upward peak at the Fe^{3+} position (which in $LuFe_2O_4$ had been attributed to a bilayer spin arrangement with all Fe^{2+} moments pointing in the field direction while two out of three bilayer Fe^{3+} moments point into the opposite direction [10,39,40]).

However, the measured $Lu_2Fe_3O_7$ crystals appear not to be as well ordered as the best crystals of $LuFe_2O_4$. No sharp features in $M(T)$ curves are observed. Furthermore, only diffuse magnetic scattering was observed in the polarized neutron scattering study (although this study was not performed on the best crystal due to its small size). Furthermore, the SO appears to be more fragile than the CO in $Lu_2Fe_3O_7$ with respect to oxygen off-stoichiometry, as the most stoichiometric available sample exhibits 3D CO in single-crystal x-ray diffraction whereas in $M(T)$ curves (Fig. 2) there are no sharp features characteristic of magnetic ordering in these materials [6,8,10]. In contrast to $LuFe_2O_4$, where competing antiferromagnetic and ferrimagnetic phases are present that differ only in the stacking of the bilayer net magnetizations [7], $M(H)$ data (Fig. 4) suggest a preference for the ferrimagnetic phase to be stabilized in $Lu_2Fe_3O_7$ as a result of the modified magnetic interactions between neighboring bilayers. The feature observed in the ZFC curves below 60 K (Fig. S1 in [31]), in which an increase of the magnetization is observed, is in disparity to $LuFe_2O_4$. This feature could be due to the ordering of the iron moments in the single layer below 60 K as suggested based on Mössbauer spectroscopy studies [22,26]. Such an ordering would be consistent with the increase of the $hh0$-correlation length deduced from the polarized neutron scattering [Fig. 9(b)].

Because of the similar arrangement of atoms and correspondingly similar superexchange interactions in the bilayers of intercalated and nonintercalated compounds, the same spin order in each individual bilayer would be expected. This is

indeed what our results from various experimental techniques indicate: (1) A net magnetic moment comparable to the saturation moment of $LuFe_2O_4$ is observed in the analysis of different macroscopic measurements $M(T)$, $M(H)$, and TRM. (2) The $\frac{1}{3}\frac{1}{3}$ in-plane propagation found in the polarized neutron study is consistent with the spin order determined in $LuFe_2O_4$ [10] and $YbFe_2O_4$ [8]. (3) The decomposition of the XMCD signal indicates the same larger Fe^{2+} net moment in field direction and smaller bilayer Fe^{3+} net moment opposite to the field as found in $LuFe_2O_4$ [10,39,40] and $YbFe_2O_4$ [8].

The principal difference of the magnetism between the intercalated and the nonintercalated compound is that in the former there is an additional contribution from the single layers. While the spins in the bilayers seem to behave as in $LuFe_2O_4$, the spins in the single Fe-O layer have no analog in $LuFe_2O_4$. Our macroscopic magnetization and XMCD results indicate a net moment of these spins that is induced by a magnetic field, paramagnetic-like in first approximation even at low temperature.

A paramagnetic-like behavior of the intercalated Fe-O single layer is not as surprising as it may seem at first glance. The Fe^{3+} ions in the single layer form a classical triangular network with antiferromagnetic nearest-neighbor interactions — this arrangement is known to be "geometrically frustrated" with a macroscopic degeneracy of possible ground states and thus a tendency for the spins to remain disordered [6,43]. In the case of the Fe-O bilayer, which shares the triangular arrangement, the degeneracy is lifted by the Fe valence dependence of the interactions and by the additional interactions between the two layers making up the bilayer, leading to the expectation of a (up to equivalence) unique ground state [44]. In contrast, lifting the geometrical frustration in the single layers rests on long-distance interactions with the neighboring bilayers. Such interactions between layers 11.8 Å apart are known to be very weak in rare-earth ferrites,

leading to the fragility of 3D order even in nonintercalated compounds [6].

However, as already noted, below about 60 K at least a partial ordering of the single-layer Fe^{3+} spins may take place as suggested both by Mössbauer spectroscopy [22,26] and by anomalies observed in the temperature dependence of neutron scattering (Fig. 9). Indeed, our polarization analysis of diffuse neutron scattering data at 4.2 K indicates a contribution of the single-layer spins: These spins seem modulated with the same in-plane propagation as the bilayer spins, but with the modulated moment in-plane rather than out-of-plane. This is consistent with an out-of-plane net moment being easily induced by an out-of-plane magnetic field as well as with the results of Mössbauer spectroscopy studies [22,26]. It shows that the magnetic interactions between bilayers and single layers, while being weak, are not negligible. For an ideal $Lu_2Fe_3O_7$ sample with perfect stoichiometry, a fully ordered ground state including all Fe spins may thus be anticipated.

Returning to the iron ions in the bilayer, we note that the similar arrangement of atoms within the bilayers in intercalated and nonintercalated compounds should also lead to similar Coulomb interactions driving charge ordering [6,45,46] and we would therefore expect not only the same spin but also the same charge order within each individual bilayer. The same CO is indeed suggested by the similar shape of the XMCD indicating the same spin-charge coupling within the bilayers [6,8,10]. Confirmation of this could be achieved by a successful solution and refinement of the charge-ordered crystal structure of $Lu_2Fe_3O_7$.

[1] J. Iida, Y. Nakagawa, and N. Kimizuka, J. Phys. Soc. Jpn. **55**, 1434 (1986).

[2] M. Inazumi, Y. Nakagawa, M. Tanaka, N. Kimizuka, and K. Siratori, J. Phys. Soc. Jpn. **50**, 438 (1981).

[3] M. Tanaka, J. Akimitsu, Y. Inada, N. Kimizuka, I. Shindo, and K. Siratori, Solid State Commun. **44**, 687 (1982).

[4] T. Mueller, Order and disorder in the charge and spin structures of $YFe_2O_{4-\delta}$ and $Ni_{0.42}Mn_{0.58}TiO_3$, Ph.D. thesis, Aachen University, 2018.

[5] N. Ikeda, K. Kohn, H. Kito, J. Akimitsu, and K. Siratori, J. Phys. Soc. Jpn. **64**, 1371 (1995).

[6] M. Angst, Phys. Status Solidi RRL **7**, 383 (2013).

[7] J. de Groot, K. Marty, M. D. Lumsden, A. D. Christianson, S. E. Nagler, S. Adiga, W. J. H. Borghols, K. Schmalzl, Z. Yamani, S. R. Bland, R. de Souza, U. Staub, W. Schweika, Y. Su, and M. Angst, Phys. Rev. Lett. **108**, 037206 (2012).

[8] H. Williamson, Spin and charge order in the newly deemed antiferroelectric $YbFe_2O_4$, Ph.D. thesis, RWTH Aachen University, 2019.

[9] H. Williamson, T. Mueller, M. Angst, and G. Balakrishnan, J. Cryst. Growth **475**, 44 (2017).

[10] J. de Groot, T. Mueller, R. A. Rosenberg, D. J. Keavney, Z. Islam, J.-W. Kim, and M. Angst, Phys. Rev. Lett. **108**, 187601 (2012).

[11] N. Ikeda, H. Ohsumi, K. Ohwada, K. Ishii, T. Inami, K. Kakurai, Y. Murakami, K. Yoshii, S. Mori, Y. Horibe, and H. Kito, Nature (London) **436**, 1136 (2005).

[12] N. Ikeda, T. Nagata, J. Kano, and S. Mori, J. Phys: Condens. Matter **27**, 053201 (2015).

[13] S. Lafuerza, J. Garcia, G. Subias, J. Blasco, K. Conder, and E. Pomjakushina, Phy. Rev. B **88**, 085130 (2013).

[14] D. Niermann, F. Waschkowski, J. de Groot, M. Angst, and J. Hemberger, Phys. Rev. Lett. **109**, 016405 (2012).

[15] A. Ruff, S. Krohns, F. Schrettle, V. Tsurkan, P. Lunkenheimer, and A. Loidl, Eur. Phys. J. B **85**, 290 (2012).

[16] S. Hammouda and M. Angst, J. Cryst. Growth **521**, 50 (2019).

[17] T. Mueller, J. de Groot, J. Strempfer, and M. Angst, J. Cryst. Growth. **428**, 40 (2015).

[18] J. de Groot, Charge, spin and orbital order in the candidate multiferroic material $LuFe_2O_4$, Ph.D. thesis, RWTH Aachen University, 2012.

[19] L. Ding, F. Orlandi, D. D. Khalyavin, A. T. Boothroyd, D. Prabhakaran, G. Balakrishnan, and P. Manuel, Crystals **8**, 88 (2018).

[20] J. Iida, M. Tanaka, and S. Funahashi, J. Magn. Magn. Mater. **104-107**, 827 (1992).

[21] N. Kimizuka, A. Takenaka, Y. Sasada, and T. Katsura, Solid State Commun. **15**, 1199 (1974).

[22] M. Tanaka, N. Kimizuka, J. Akimitsu, S. Funahashi, and K. Siratori, J. Magn. Magn. Mater. **31-34**, 769 (1983).

[23] M. Tanaka and J. Iida, Hyperfine Interact. **84**, 217 (1994).

[24] H. Yang, Y. Zhang, Y. Qin, C. Ma, H. Tian, and J. Li, Phys. Status Solidi (b) **247**, 870 (2010).

[25] K. Yoshii, N. Ikeda, R. Fukuyama, T. Nagata, T. Kambe, Y. Yoneda, T. Fukuda, and S. Mori, Solid State Commun. **173**, 34 (2013).

[26] T. Sugihara, K. Siratori, N. Kimizuka, J. Iida, H. Hiroyoshi, and Y. Nakagawa, J. Phys. Soc. Jpn. **54**, 1139 (1985).

[27] Y. Qin, H. Yang, L. Wang, H. Tian, C. Ma, Y. Li, H. Shi, and J. Li, Eur. Phys. J. B **75**, 231 (2010).

[28] Y. Fukada, R. Fukuyama, K. Fujiwara, K. Yoshii, K. Shigematsu, M. Azuma, and N. Ikeda, J. Phys. Soc. Jpn. **90**, 024710 (2021).

[29] M. Tanaka, Nucl. Instrum. Methods Phys. Res., Sect. B **76**, 149 (1993).

[30] Y. Su, K. Nemkovskiy, and S. Demirdiş, J. Large-Scale Res. Facil. **1**, A27 (2015).

[31] See Supplemental Material at http://link.aps.org/supplemental/10.1103/PhysRevB.104.174437 for additional M vs T data on crystal SC3 and on $LuFe_2O_4$, and for O K edge x-ray absorption spectroscopy.

[32] X. S. Xu, M. Angst, T. V. Brinzari, R. P. Hermann, J. L. Musfeldt, A. D. Christianson, D. Mandrus, B. C. Sales, S. McGill, J. W. Kim, and Z. Islam, Phys. Rev. Lett. **101**, 227602 (2008).

[33] M. Phan, N. Frey, M. Angst, J. de Groot, B. C. Sales, D. Mandrus, and H. Srikanth, Solid State Commun. **150**, 341 (2010).

[34] M. K. Chattopadhyay, S. B. Roy, and P. Chaddah, Phys. Rev. B **72**, 180401(R) (2005).

[35] J. Moore, G. Perkins, K. Morrison, L. Ghivelder, M. Chattopadhyay, S. Roy, P. Chaddah, K. Gschneidner, Jr., V. Pecharsky, and L. Cohen, J. Phys.: Condens. Matter **20**, 465212 (2008).

[36] T. Brückel, S. Förster, G. Roth, and R. Zorn (eds), *Laboratory Course Neutron Scattering – Lectures*, Schriften des Forschungszentrums Jülich. Reihe Schlüsseltechnologien / Key Technologies, Vol. 147 (Forschungszentrum Jülich GmbH Zentralbibliothek, Verlag, Jülich, Germany, 2017).

[37] A. D. Christianson, M. D. Lumsden, M. Angst, Z. Yamani, W. Tian, R. Jin, E. A. Payzant, S. E. Nagler, B. C. Sales, and D. Mandrus, Phys. Rev. Lett. **100**, 107601 (2008).

[38] S. Blundell, *Magnetism in Condensed Matter* (Oxford University Press, Oxford, 2001).

[39] K. Kuepper, M. Raekers, C. Taubitz, M. Prinz, C. Derks, M. Neumann, A. V. Postnikov, F. M. F. de Groot, C. Piamonteze, D. Prabhakaran, and S. J. Blundell, Phys. Rev. B **80**, 220409(R) (2009).

[40] K. T. Ko, H. J. Noh, J. Y. Kim, B. G. Park, J. H. Park, A. Tanaka, S. B. Kim, C. L. Zhang, and S. W. Cheong, Phys. Rev. Lett. **103**, 207202 (2009).

[41] S. Lafuerza, J. García, G. Subías, J. Blasco, J. Herrero-Martín, and S. Pascarelli, Phys. Rev. B **90**, 245137 (2014).

[42] J. Iida, M. Tanaka, Y. Nakagawa, S. Funahashi, N. KimizukaI, and S. Takekawa, J. Phys. Soc. Jpn. **62**, 1723 (1993).

[43] R. Moessner and A. P. Ramirez, Phys. Today **59**(2), 24 (2006).

[44] H. J. Xiang, E. J. Kan, S.-H. Wei, M.-H. Whangbo, and J. Yang, Phys. Rev. B **80**, 132408 (2009).

[45] Y. Yamada, K. Kitsuda, S. Nohdo, and N. Ikeda, Phys. Rev. B **62**, 12167 (2000).

[46] A. B. Harris and T. Yildirim, Phys. Rev. B **81**, 134417 (2010).